IEEE Access
Multidisciplinary | Rapid Review | Open Access Journal

Received 23 June 2024, accepted 5 July 2024, date of publication 11 July 2024, date of current version 23 July 2024.

Digital Object Identifier 10.1109/ACCESS.2024.3426488

RESEARCH ARTICLE

Modeling, Simulation, and Design of Electromagnetic Capacity Control System for Reciprocating Compressors

DEGENG ZHAO[1,2], YAO WANG[1,2], JINJIE ZHANG[1,2,3], AND ZHINONG JIANG[1,2,3]

[1]Beijing Key Laboratory of High-End Mechanical Equipment Health Monitoring and Self-Recovery, Beijing University of Chemical Technology, Beijing 100029, China
[2]National Key Laboratory of High-End Compressor and System Technology, Beijing University of Chemical Technology, Beijing 100029, China
[3]Key Laboratory of Engine Health Monitoring-Control and Networking, Ministry of Education, Beijing University of Chemical Technology, Beijing 100029, China

Corresponding author: Yao Wang (wy@mail.buct.edu.cn)

This work was supported in part by the National Natural Science Foundation of China under Grant 52101343, and in part by the Fundamental Research Funds for the Central Universities under Grant ZY2455.

ABSTRACT Designing an efficient and simplified electromagnetic capacity control system (ECCS) for reciprocating compressors, replacing hydraulic systems, is a crucial focus for energy conservation and efficiency enhancement in industrial production. Major challenges lie in the compressor's high gas force and rotational speed, coupled with the actuator coil's self-inductance, leading to complex response characteristics and capacity control failures under traditional on-off drive modes. To address these issues, this paper introduces a coupling control model for capacity control under synchronous frequency with asynchronous actuation of the actuator and suction valve, considering periodic excitation, reverse attraction, and partial stroke contact. By simulating actuator response and compressor performance under various voltage drives, as well as conducting a sensitivity analysis of various control parameters, we develop a load regulation procedure using Fixed Duration Timing Shift and Variable Duration (FDTSVD). This procedure achieves precise 0%-100% load regulation, with discharge volume relative error $<7.5\%$. When the exhaust load decreases from 100 % to 25 %, the one-cycle indicated work decreases from 593.6 J to 175.2 J, demonstrating its effectiveness.

INDEX TERMS Capacity control, electromagnetic actuator, coupling model, dynamic simulation.

I. INTRODUCTION

As critical dynamic equipment in industrial production, reciprocating compressor systems transport high-pressure raw material gas media to production processes, serving as a crucial node in the material flow of industrial production. Historically, compressor systems have incurred significant energy consumption [1]. With various issues of overcapacity, mismatches between initial process design and market demands, and increasingly prominent contradictions in production factor allocation, it is typically necessary to adjust the compressor capacity to meet varying loads [2], [3].

Considerable research has been done on the capacity control of reciprocating compressors, and various control schemes have been proposed, such as bypass control [4], switching cycle control [5], unloading cylinder control [6], and so on. However, there are some shortcomings, such as low control efficiency, easy to wear the compressor, limited control range, and uneven force, which limit the application of the above technology. In recent years, the rapid development of the capacity control system (CCS) based on the delayed closure of suction valves has shown significant progress, offering superior energy-saving effects [7]. Several scholars

The associate editor coordinating the review of this manuscript and approving it for publication was Hassen Ouakad.

have conducted in-depth research on the CCS, resulting in significant achievements. Hong et al. [8] established a theoretical model for step-less capacity control conditions in reciprocating compressors, obtained the thermal cycle patterns under different load conditions, and validated the model through experimental testing on a prototype. Liu et al. [9] analyzed relevant parameters of the hydraulic system, such as the orifice size of the electromagnetic valve and piston diameter, and their impact on the operation of the suction valve. Xu and Hong [10] examined the dynamic performance variations in comprehensive piston force, connecting rod force, crankshaft tangential force, and normal force of the reciprocating compressor under different load conditions. Wang et al. [11] obtained relatively reasonable hydraulic pressure, displacement, and retraction speed of the mechanical actuator by analyzing the impact of hydraulic pressure, displacement, and speed on compressor performance. Yang et al. [12] proposed a rapid algorithm to calculate the gas pulsations in CCS and further incorporated it into the frequency domain modeling of gas pulsations. Sun et al. [13] established a multi-platform joint simulation model, improving upon traditional independent modeling methods for single systems. They conducted an analysis of compressor performance under variable capacity control conditions and explored the optimization of control parameters.

It should be noted that the existing research on capacity control techniques based on the principle of delayed suction valve closure predominantly relies on hydraulic systems as the driving force. While achieving good control effects, there are issues such as system complexity, high cost, and inevitable oil contamination, making engineering application and maintenance challenging. Some scholars have proposed new methods for capacity control based on electromagnetic drive, which can effectively address the aforementioned problems. However, there is a lack of relevant simulation models for the analysis of the characteristics of electromagnetic capacity control systems, and the research on multi-parameter coupling laws and related system maturity is still limited.

ECCS replaces hydraulic force with electromagnetic force to drive the suction valve unloading device to perform ejection and retraction motion. As the reciprocating compressor suction valve unloading device is subject to significant forces, including gas force and spring force, the electromagnetic actuator not only needs to have a large driving force but also must meet the requirements of rapid motion. The design of the electromagnetic actuator coil turns needs to be relatively large to produce a strong self-inductance effect. This directly affects its dynamic characteristics, leading to compressor capacity control failure. Electromagnetic actuators are widely used in various valve control areas, and relevant research can provide us with references. For example, Naseradinmousavi and Nataraj [14] derived a coupled model of electromagnetic dynamics, fluid dynamics, and mechanical dynamics through some simplified assumptions. The results show that the characteristics of fluid dynamic torque play an important role in the process of valve closing and opening. Yuan et al. [15] integrated electrical, electromagnetic, fluid dynamic, and mechanical models to achieve an analytical and fully coupled mathematical model, effectively capturing the nonlinear dynamic performance determined by structural parameters, materials, fluids, driving strategies, and subsystem interactions. Paden et al. [16] proposed a novel electromechanical valve actuation system consisting of an electromagnetic actuator, a valve, and a storage cam/spring mechanism. Modeling and control strategies were designed to enable the valve to achieve sufficiently fast transitions between open and closed positions. Wu et al. [17] optimized parameters by establishing an analytical model, improving the static characteristics and dynamic step response of high-speed switching valves. These studies provide good references for modeling the electromagnetic capacity control system of reciprocating compressors. However, the inherent characteristics of the CCS itself should be taken into account during modeling, such as the coupling problems caused by the asynchronous working mode of the electromagnetic actuator and the suction valve at the same frequency, the periodic excitation characteristics of the electromagnetic actuator, the reverse pull-in situation of the electromagnetic actuator, and the partial stroke contact characteristics of the actuator and the suction valve during the retract process. These are important for the accuracy of the model and should be fully considered.

This paper establishes a mathematical model for the ECCS of reciprocating compressors with multi-system coupling. To ensure the accuracy of the model, the periodic characteristics of the excitation signal, the reverse attraction of the actuator, and the partial stroke contact characteristics of the actuator and the suction valve during the retracting process are considered. Based on this model, the influence of different driving modes and control parameters on the capacity control performance is simulated and analyzed. Based on the simulation data and FDTSVD method, the load control calculation program is designed. It can realize 0 % -100 % load regulation of the compressor. The load regulation experiment was carried out and good results were achieved.

The main contributions and innovations of this paper can be summarized as follows:

1) This paper introduces a coupling control model for capacity control by asynchronously driving the actuator and suction valve at synchronous frequency, establishing a working principle model for ECCS that comprehensively considers factors such as periodic excitation, reverse attraction, and partial stroke contact.
2) By simulating the actuator response and compressor performance under different voltage drives, this paper has developed a load regulation procedure based on FDTSVD.
3) This paper has developed an efficient and simplified experimental setup for the ECCS, validating the effectiveness of the theoretical model and control method. It has been proven that the ECCS can effectively replace the hydraulic capacity control system (HCCS)

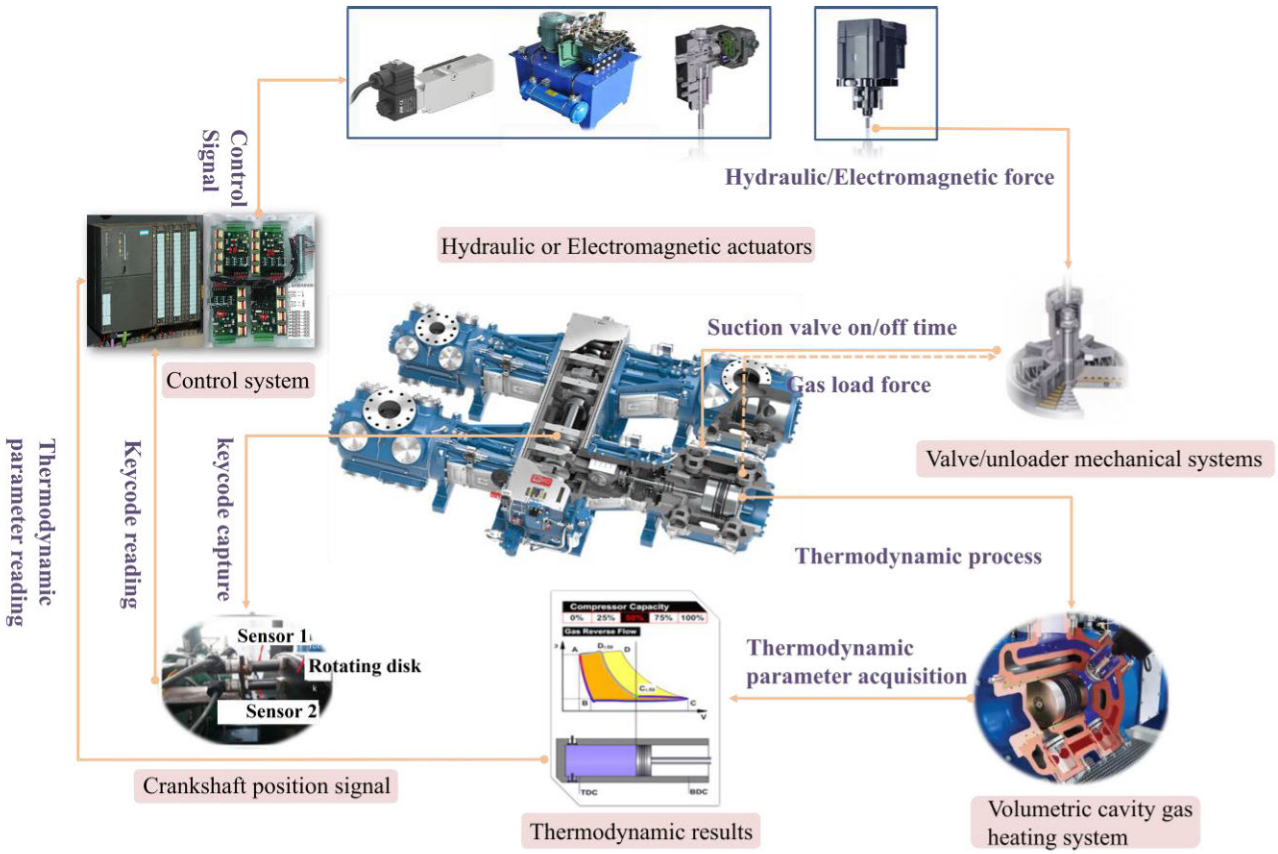

FIGURE 1. Stepless CCS of the reciprocating compressor.

in compressors, achieving energy conservation and efficiency enhancement.

II. COMPOSITION AND WORKING PRINCIPLES OF CCS

The CCS of a reciprocating compressor consists of the driving system, control system, mechanical execution mechanism, and monitoring system, as illustrated in Fig. 1. According to the type of actuation, CCS can be categorized into HCCS, which is driven by hydraulic actuators, and ECCS, which is driven by electromagnetic actuators. The hydraulic execution mechanism is powered by the hydraulic system. It controls the duration of hydraulic pressure by toggling high-speed electromagnetic valves. The electromagnetic execution mechanism generates different magnitudes of electromagnetic force by directly controlling the magnitude and time of excitation voltage. ECCS greatly simplifies the system and avoids the risk of oil leakage due to the elimination of components such as oil stations and pipelines. Typically, each valve of the compressor is equipped with a set of mechanical execution mechanisms.

The components of the CCS are interdependent, with strong correlations between various parameters, collectively influencing the operational performance of the compressor. Therefore, it is necessary to establish a multi-system coupled analytical model to enhance computational efficiency and accurately reflect the patterns of parameter variations within the system.

III. WORKING PRINCIPLE MODEL OF THE ECCS

For the convenience of model construction, this paper makes the following assumptions in the modeling process, drawing on previous research:

1) The compression process is considered to be adiabatic [18];
2) The pressure at the end of the reflow is approximated as the suction pressure;
3) The magnetic permeability is assumed to be a constant value, and the magnetic flux in the magnetic circuit is mainly attenuated at each air gap [19];
4) The coil inductance after magnetization is neglected [20].

A. CALCULATION MODEL FOR DISCHARGE VOLUME AND LOAD RATIO

The relationship between the piston motion stroke h and the crankshaft angle θ for a reciprocating compressor is as follows:

$$h = r(1 - \cos\theta) + l(1 - \sqrt{1 - \frac{r^2}{l^2}\sin^2(\theta)}) \qquad (1)$$

where r is the radius of the crank, and l denotes the length of the connecting rod, as shown in Fig. 2.

The discharge volume Q_v equals the volume of the compression chamber V_{ADV} when the discharge valve just opens

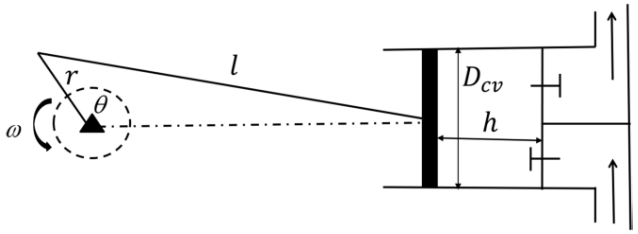

FIGURE 2. The main moving parts of reciprocating compressor and the geometric relationship between them.

minus the clearance volume V_0.

$$Q_v = V_{ADV} - V_0 \tag{2}$$

When the backflow ends, the remaining gas volume in the compression chamber V_{ASV} undergoes the compression process to obtain the volume V_{ADV}. This process is considered an adiabatic process, and if we approximate the pressure at the end of backflow as the suction pressure, then:

$$V_{ADV} = V_{ASV}(\frac{p_s}{p_d})^{\frac{1}{k_e}} \tag{3}$$

where p_s is the suction pressure, p_d denotes the discharge pressure, and k_e is the adiabatic process coefficient. The remaining gas volume in the compression chamber after backflow V_{ASV} can be determined by the piston stroke volume V_h and clearance volume V_0:

$$V_{ASV} = V_h + V_0 \tag{4}$$

The piston stroke volume V_h is determined by the piston cross-sectional area and the motion stroke:

$$V_h = \frac{\pi D_{cv}^2}{4} \cdot h \tag{5}$$

where D_{cv} is the diameter of the piston.

By combining the above equations, the calculation model for the discharge volume of a reciprocating compressor under capacity control is as follows:

$$Q_v = \Gamma(\theta_{bf}) = \begin{bmatrix} \frac{\pi D_{cv}^2}{4} r(1-\cos(\theta_{bf}) + \\ \frac{l}{r}(1-\sqrt{1-\frac{r}{l}^2 \sin^2(\theta_{bf})})) \\ -V_0((\frac{p_d}{p_s})^{\frac{1}{k_e}} - 1) \end{bmatrix} \cdot (\frac{p_s}{p_d})^{\frac{1}{k_e}} \tag{6}$$

When operating at full load without backflow, the discharge volume of a reciprocating compressor is as follows:

$$Q_{100\%} = \Gamma(\pi) = \begin{bmatrix} \frac{\pi D_{cv}^2}{4} r(1-\cos(\pi) + \\ \frac{l}{r}(1-\sqrt{1-\frac{r}{l}^2 \sin^2(\pi)})) \\ -V_0((\frac{p_d}{p_s})^{\frac{1}{k_e}} - 1) \end{bmatrix} \cdot (\frac{p_s}{p_d})^{\frac{1}{k_e}} \tag{7}$$

The load ratio is defined as follows:

$$\eta = \frac{Q_v}{Q_{100\%}} \times 100\% \tag{8}$$

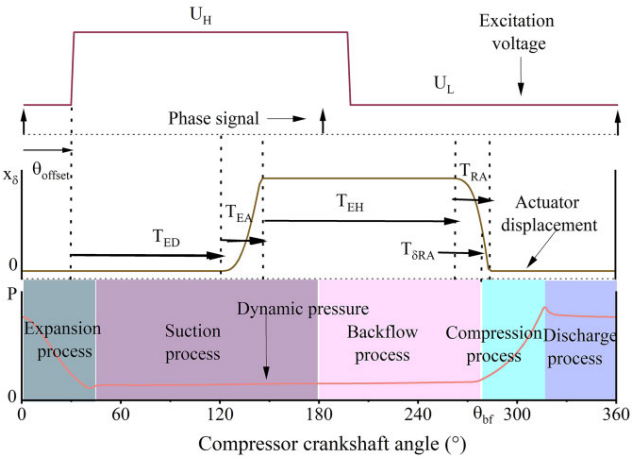

FIGURE 3. Actuator response principles and illustration of coupling action parameters.

B. ANALYSIS OF THE COUPLING RELATIONSHIP BETWEEN THE ACTUATOR AND THE COMPRESSOR

As shown in Fig. 3, the capacity control with delayed suction valve closure mainly includes the following operation processes:

1) The actuator receives the driving signal at a certain time in a cycle of the compressor, and the crankshaft produces a phase signal at each half-turn. The deviation angle of the driving signal starting time relative to the phase signal is defined as the key phase offset angle θ_{offset}.
2) After receiving the drive signal, the electromagnetic force begins to increase until it overcomes the load force to complete the ejection action. The time elapsed from the initiation of the drive voltage signal to the beginning of the ejection is defined as the ejection delay time T_{ED}. This characterizes the process of the electromagnetic force growing from its initial value to the critical load force for ejection.
3) Subsequently, the actuator begins its action, and the time taken for the action process is defined as the ejection action time T_{EA}.
4) After the actuator completes the ejection, it acts upon the suction valve, compelling it to remain open for a specific duration. This period is defined as the ejection hold time T_{EH}.
5) When the electromagnetic force decreases to the critical load value for retraction, the actuator begins to retract. The time taken for the retraction action process is defined as T_{RA}.

During the retraction process, the actuator and the compressor suction valve remain in place for only a period throughout the process. Even after the valve reaches the closed limit position, the actuator continues to move for a certain distance. At this point, the contact coefficient $\delta = \sqrt{\frac{x_{valve}}{x_\delta}}$ is defined. The duration of the interaction between the actuator and the valve during the retraction process is as

follows:

$$T_{\delta RA} = \delta \cdot T_{RA} \tag{9}$$

where x_{valve} is the stroke displacement of the suction valve, while x_δ denotes the actuator's stroke displacement.

Establishing the coupling relationship between the actuator action parameters during the periodic response and the phase angle of the reciprocating compressor backflow, based on the time parameters of the aforementioned five working processes, is outlined as follows:

$$\theta_{bf} = \theta_{offset} + (T_{ED} + T_{EA} + T_{EH} + T_{\delta RA}) \cdot 2\pi f_n \tag{10}$$

where f_n is the frequency of the actuator's action, which is determined by the compressor's rotational speed parameters.

Furthermore, it is essential to consider two dynamic behaviors of the actuator when it fails to respond cyclically: the inability to retract after ejection and the failure to eject. These behaviors are determined by the relative relationship between the electromagnetic driving force and the load force. In such cases, the overall coupling relationship between the electromagnetic actuator and the phase angle of the reciprocating compressor backflow is as follows:

$$\theta_{bf} = \begin{cases} \pi, (F_{\max} \leq F_{load\,\min}) \\ 2\pi, (F_{\min} \geq F_{load\,\max}) \\ \theta_{offset} + (T_{ED} + T_{EA} + T_{EH} + T_{\delta RA}) \cdot 2\pi f_n \\ (F_{\max} \succ F_{load\,\max}, F_{\min} \prec F_{load\,\min}) \end{cases} \tag{11}$$

From equation (11), it can be observed that to solve the coupling relationship, the following tasks need to be performed:

(1) Solve for different response state boundary conditions.

(2) Calculate different time parameters for the electromagnetic actuator action.

The action parameters of the electromagnetic actuator, T_{ED} and T_{EH}, represent the time for the electromagnetic force to change when the actuator is in a stationary state. The parameters T_{EA} for ejection action and T_{RA} for retraction action represent the time the actuator spends in the action states. The action state time parameters need to be solved by establishing the motion equation of the actuator:

Ejection action state:

$$\begin{cases} \dfrac{dx}{dt} = v_E \\ m\dfrac{dv_E}{dt} = F_m - F_{load} - F_{friction} \end{cases} \tag{12}$$

Retraction action state:

$$\begin{cases} \dfrac{dx}{dt} = v_R \\ m\dfrac{v_R}{dt} = F_{load} - F_m - F_{friction} \end{cases} \tag{13}$$

where v_E represents the velocity variation during the actuator's ejection process, v_R denotes the velocity variation during the actuator's retraction process, F_m denotes the electromagnetic force, F_{load} represents the load force, and $F_{friction}$ refers to the frictional force encountered during the motion process.

Based on the motion equations (12) and (13) for ejection and retraction, the solution for the ejection and retraction action time is as follows:

$$\begin{cases} T_{EA} = \displaystyle\int_0^{|v_{E\max}|} \frac{m.dv}{F_m - F_{load} - F_{friction}} \\ T_{RA} = \displaystyle\int_0^{|v_{R\max}|} \frac{m.dv}{F_{load} - F_m - F_{friction}} \end{cases} \tag{14}$$

where $v_{E\max}$ is defined as the maximum motion velocity during the ejection process, $v_{E\max} = Max(v_E)$; $v_{R\max}$ is the maximum motion velocity during the retraction process, $v_{R\max} = Max(v_R)$.

Ejection delay time T_{ED} and ejection holding time T_{EH} characterize the time for the electromagnetic force to change in a stationary state. The change in electromagnetic force in a stationary state is only related to the current. Therefore, the solution can be based on the relationship between the time parameters of the action and the current [21].

$$T = \frac{L}{R}\ln\left(\frac{U - I_{t_0}R}{U - I_{t_1}R}\right) \tag{15}$$

where I_{t_0} is the current at the initial moment of a certain process, I_{t_1} represents the current at the end of the process, and U represents the magnitude of the excitation voltage as the current changes from time t_0 to time t_1, while R and L denoting the coil resistance and inductance, respectively.

Defining the current value at the initial energization moment as I_0 and the critical current value at the onset of actuator motion as I_{FL1}. Considering the reverse attraction situation when U_L is not zero, the driving voltage during the ejection process in positive attraction is U_H. In the case of reverse attraction, the driving voltage during the ejection process is U_L. Therefore, the calculation of the ejection delay time is as follows:

$$T_{ED} = \begin{cases} \dfrac{L}{R}\ln\left(\dfrac{U_H - I_0R}{U_H - I_{FL1}R}\right) & I_\phi \succ 0 \\ \dfrac{L}{R}\ln\left(\dfrac{U_L - I_0R}{U_L - I_{FL1}R}\right) & I_\phi \prec 0 \end{cases} \tag{16}$$

Defining the critical current value after ejection as I_{FL2} and the critical current at the onset of retraction as I_{FL3}, the current transition from I_{FL2} to I_{FL3} is not a simple process; it undergoes an initial rise followed by a decrease. Further, defining the maximum absolute current value during the ejection holding process as I_ϕ, where the current first changes from I_{FL2} to I_ϕ and then from I_ϕ to I_{FL3}. Considering both positive and reverse attraction scenarios, the ejection hold time T_{EH} is calculated as follows:

$$T_{EH} = \begin{cases} \dfrac{L}{R}\ln\left(\dfrac{U_H - I_{FL2}R}{U_H - I_\phi R}\right) + \dfrac{L}{R}\ln\left(\dfrac{U_L - I_\phi R}{U_L - I_{FL3}R}\right) & I_\phi \succ 0 \\ \dfrac{L}{R}\ln\left(\dfrac{U_L - I_{FL2}R}{U_L - I_\phi R}\right) + \dfrac{L}{R}\ln\left(\dfrac{U_H - I_\phi R}{U_H - I_{FL3}R}\right) & I_\phi \prec 0 \end{cases} \tag{17}$$

Equations (16) and (17) can be further expanded. When the number of voltage segments in each process increases, it is only necessary to define the initial and final current values under each voltage segment, and then sequentially calculate and solve.

Based on the above analysis, it is evident that solving the coupling relationship between the electromagnetic actuator and the phase of the compressor backflow under different response states requires the construction of an integrated model that links the actuator's driving voltage, operating current, and electromagnetic driving force. This model aims to capture the variations in operating current and electromagnetic driving force, then solve the time parameter.

By utilizing the electromagnetic driving force model, the solution involves determining the response boundary conditions and action characteristic parameters T_{EA} and T_{RA}. Simultaneously, the working current model is employed to solve for the defined characteristic current values $I_0, I_{\phi}, I_{FL1}, I_{FL2}$, and I_{FL3}.

C. ESTABLISHMENT OF ELECTROMAGNETIC ACTUATOR RESPONSE MODEL

The CCS in a reciprocating compressor, which involves delayed closure of the intake valve, requires the implementation of unloader ejection and retraction actions in each working cycle. Therefore, the control signal for this process is cyclically driven. Periodic signals are often represented by piecewise functions, which exhibit simple and intuitive characteristics. However, solving transient currents can be challenging, especially when the periodic signal is complex, as shown in Fig. 4. This difficulty hinders the subsequent construction and solution of models and complicates the analysis of coupling between parameters. To address this, this section establishes an analytical expression for an n-segment periodic signal based on the Fourier series [22], [23], and the current response model under periodic signal excitation is solved, which provides a basis for subsequent model development and parameter analysis.

Given the satisfaction of Dirichlet conditions, a non-sinusoidal periodic voltage $U(t)$ with a period of T can be expanded into a Fourier series as follows:

$$U(t) = A_0 + \sum_{k=1}^{+\infty} [A_k \cos k\omega t + B_k \sin k\omega t] \tag{18}$$

The non-sinusoidal periodic voltage source can be regarded as a direct current (DC) voltage source combined with numerous sinusoidal alternating current (AC) sources of varying frequencies, all working together within the electrical circuit.

The actuator coil and the power supply can be regarded as an equivalent RL circuit, The design of electromagnetic actuator and the transformation of subsystem parameters are shown in Fig. 5. According to Kirchhoff's voltage law, the following expression can be obtained:

$$U(t) = L\frac{di}{dt} + Ri(t) + k_f\frac{dx}{dt} \tag{19}$$

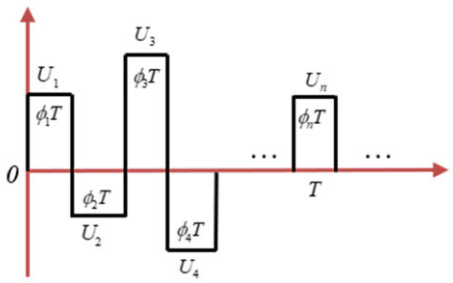

FIGURE 4. n-segment voltage profile illustration.

where k_f represents the coefficient of induced electromotive force, x stands for the displacement of the armature.

Through the Fourier series expansion and the orthogonality of the trigonometric function, the transient current and the expansion coefficient A_0, A_k, B_k are solved as (20) and (21), shown at the bottom of the next page [24].

The equivalent magnetic circuit schematic of the electromagnetic actuator is shown in Fig. 6. Assuming that the magnetic permeability is a constant value and the magnetic circuit flux φ decays mainly at each air gap, the total internal magnetoresistance of the electromagnet is as follows:

$$\begin{cases} R(x) = \sum_{i=1}^{n} R_{mi} + \sum_{i=1}^{3} R_{gi} = \sum_{i=1}^{3} R_{gi} \\ R_i = \dfrac{l_i}{\mu_i A_i} \end{cases} \tag{22}$$

where R_i is the i reluctance; m stands for the magnetic conductor, g stands for the air gap; l_i is the equivalent length of the i reluctance circuit;A_i is the cross-sectional area of the i circuit; μ_i is the permeability of the i reluctance circuit. The magnitude of magnetic flux in the magnetic circuit is as follows:

$$\varphi = \frac{Ni(t)}{R(x)} \tag{23}$$

where N is the number of turns of the coil.

Considering the nonlinear, time-varying characteristics of the coil inductance, the coil inductance after neglecting the magnetization can be expressed as follows:

$$L(x) = \frac{N^2}{R(x)} \tag{24}$$

The magnitude of the magnetic induction of the air gap at work:

$$B_g = \frac{\varphi}{s_{g1}} \tag{25}$$

where s_{g1} is the working air gap area.

Then the expression of electromagnetic force is as follows:

$$F_m = \frac{B_g^2 s_{g1}}{2\mu_0} = \frac{N^2 i(t)^2}{2\mu_0 R(x)^2 s_{g1}} \tag{26}$$

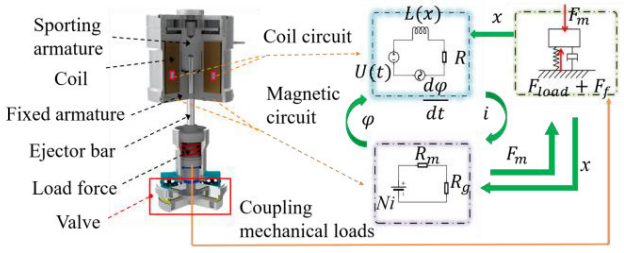

FIGURE 5. Electromagnetic actuator structure and equivalent RL circuit schematic.

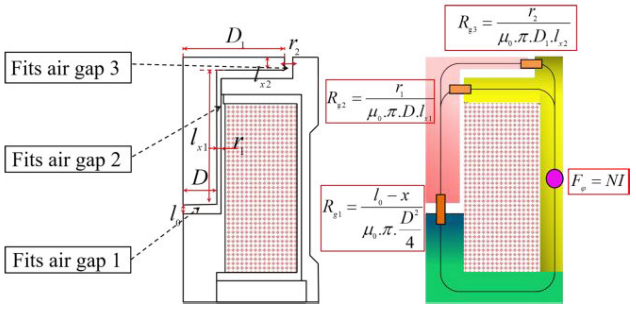

FIGURE 6. Key structural parameters and equivalent magnetic circuit diagram of electromagnetic actuator.

D. FEATURE PARAMETER SOLUTION

Using the established electromagnetic actuator response model, the solution of the characteristic parameters in the previous coupling relationship is obtained. I_0 and I_ϕ respectively represent the current at the onset of high-level excitation and the corresponding current at the onset of low-level excitation. With the known control parameters, I_0 and I_ϕ are obtained through (20).

$$\begin{aligned} I_0 &= i(t)_{t=0+\xi T,\xi=0,1,2\ldots} \\ I_\phi &= i(t)_{t=T_\phi+\xi T,\xi=0,1,2\ldots} \end{aligned} \tag{27}$$

I_{FL1}, I_{FL2}, and I_{FL3} are obtained through force balance analysis during the moments of actuator state transitions. The critical force condition for the actuator to open the intake valve, transitioning from a stationary state to the initiation of the ejection motion, is given by $F_m = F_{load} + F_{friction}$. At this point, the critical current I_{FL1} can be calculated as follows, based on (26).

$$I_{FL1} = \begin{cases} \dfrac{R(x)}{N}\sqrt{(F_{load}+F_{friction})2\mu_0 s_{g1}}\,|x=0 & I_\phi \succ 0 \\ -\dfrac{R(x)}{N}\sqrt{(F_{load}+F_{friction})2\mu_0 s_{g1}}\,|x=0 & I_\phi \prec 0 \end{cases} \tag{28}$$

Similarly, the conditions for the actuator to retract and the valve to close are: $F_{load} - F_{friction} = F_m$, when the actuator is just completely ejected or begins to retract, the force conditions areessentially identical. At this moment, according to (26), the critical currents I_{FL2}, I_{FL3}

$$i(t) = \begin{bmatrix} \frac{-1}{R}\cdot e^{\frac{R}{L}.t} & \sum_{k=1}^{+\infty}\frac{-A_k}{S}\cdot e^{\frac{-R}{L}.t} & \sum_{k=1}^{+\infty}\frac{B_k}{S}\cdot e^{\frac{-R}{L}.t} \\ \frac{1}{R} & 0 & 0 \\ 0 & \sum_{k=1}^{+\infty}\frac{A_k}{S}\cdot\cos k\omega t & \sum_{k=1}^{+\infty}\frac{-B_k}{S}\cdot\cos k\omega t \\ 0 & \sum_{k=1}^{+\infty}\frac{B_k}{S}\cdot\sin k\omega t & \sum_{k=1}^{+\infty}\frac{A_k}{S}\cdot\sin k\omega t \end{bmatrix} \cdot \begin{bmatrix} A_0 - k_f\frac{dx}{dt} \\ R \\ k\omega L \end{bmatrix} \tag{20}$$

$$\begin{cases} A_0 = \dfrac{1}{T}\cdot\int_0^{\phi_1 T} U_1 dt + \dfrac{1}{T}\cdot\int_{\phi_1 T}^{(\phi_1+\phi_2)T} U_2 dt + \ldots + \dfrac{1}{T}\cdot\int_{\sum_{i=1}^{n-1}\phi_i T}^{\sum_{i=1}^{n}\phi_i T} U_n dt \\ A_k = \frac{2}{T}\cdot\int_0^{\phi_1 T} U_1\cdot\cos(k\omega t)dt + \\ \frac{2}{T}\cdot\int_{\phi_1 T}^{(\phi_1+\phi_2)T} U_2\cdot\cos(k\omega t)dt + \ldots + \frac{2}{T}\cdot\int_{\sum_{i=1}^{n-1}\phi_i T}^{\sum_{i=1}^{n}\phi_i T} U_n\cdot\cos(k\omega t)dt \\ B_k = \frac{2}{T}\cdot\int_0^{\phi_1 T} U_1\cdot\sin(k\omega t)dt + \\ \frac{2}{T}\cdot\int_{\phi_1 T}^{(\phi_1+\phi_2)T} U_2\cdot\sin(k\omega t)dt + \ldots + \frac{2}{T}\cdot\int_{\sum_{i=1}^{n-1}\phi_i T}^{\sum_{i=1}^{n}\phi_i T} U_n\cdot\sin(k\omega t)dt \\ S = R^2 + (k\omega L)^2 \end{cases} \tag{21}$$

can be calculated as follows:

$$I_{FL2} = I_{FL3} = \begin{cases} \frac{R(x)}{N}\sqrt{(F_{load} - F_{friction})2\mu_0 s_{g1}}\,|x = x_\delta & I_\phi \succ 0 \\ -\frac{R(x)}{N}\sqrt{(F_{load} - F_{friction})2\mu_0 s_{g1}}\,|x = x_\delta & I_\phi \prec 0 \end{cases} \tag{29}$$

IV. SIMULATION ANALYSIS

This section, building upon the model established in Section III, focuses on exploring the driving modes and capacity control methods of ECCS through simulation. It specifically investigates the two commonly used driving methods for electromagnetic actuators: single-voltage drive and dual-voltage drive [25].

A. SIMULATION PARAMETER CONFIGURATION

The paper utilizes a DC electromagnet of the SDT-158153S126A40 specification from the laboratory, and the DW-12/2 model compressor as case studies for the research. By measuring the key structural dimensions depicted in Figs. 2 and 4, the simulation setup data has been derived as illustrated in Tables 1 and 2.

B. ANALYSIS OF CAPACITY CONTROL EFFECT IN SINGLE-VOLTAGE DRIVE MODE

The illustration of the On/Off control signal in the single-voltage mode is shown in Fig. 5, where $T_{\phi 1}$ represents the duration of the power-on period within one cycle, $T_{\phi 2}$ represents the duration of the power-off period within one cycle, and the sum of these two times represents the period length of the excitation signal, i.e., $T = T_{\phi 1} + T_{\phi 2}$. The period length T of the excitation signal is determined by the compressor speed parameter, and with the specified speed parameter of 300 rpm in Table 2, the period $T = \frac{60000}{300} = 200ms$, under the On/Off control mode, is $n = 2$, $U_2 = 0$.

Using (21), we obtained the three expansion coefficients as follows:

$$\begin{cases} A_0 = U_1.\phi_1 \\ A_k = \dfrac{\sin(2k\pi\phi_1)}{k.\pi}.U_1 \\ B_k = \dfrac{1-\cos(2k\pi\phi_1)}{k.\pi}.U_1 \\ \phi_1 = \dfrac{T_{\phi 1}}{T} \end{cases} \tag{30}$$

1) ANALYSIS OF MULTI-CYCLE RESPONSE PROCESS FOR ELECTROMAGNETIC FORCE AND LOAD FORCE

The load force is mainly provided by the spring force. When the actuator is not ejected, the spring pre-compression force is 450 N. When the actuator is completely ejected, the spring load force is 750 N. The electromagnetic actuator has a rated voltage of 220V. Fig. 8 illustrates the variation patterns of electromagnetic force and load force over 25 cycles under the excitation of the rated voltage. The power-on duration $T_{\phi 1}$ for each cycle is set to 10ms, 20ms, and 30ms, respectively.

TABLE 1. Electromagnetic actuator parameters.

Name	Value
Number of coils N	4100
Coil resistance R (Ω)	40
Armature diameter D (mm)	50
Diameter of armature disc D_l (mm)	90
The thickness of the armature disc l_{x2} (mm)	5
Working air gap length l_0 (mm)	6
Armature and coil mating length l_{x1} (mm)	60
Armature and coil mating thickness r_l (mm)	2
The size of the air gap between the armature disc and the shell r_2 (mm)	5
Rated voltage (V)	220

From the graph, it can be observed that in the multi-cycle response scenario, regardless of the duration of the power-on period for each cycle, the electromagnetic force undergoes both transient and steady-state processes. The variation in electromagnetic force generally enters a steady state around the 10th cycle. Before the 10th cycle, the maximum ($F_{\max} = \mathrm{Max}(F_m)$) and minimum ($F_{\min} = \mathrm{Min}(F_m)$) values of the electromagnetic force change continuously within each cycle. After the 10th cycle, the maximum and minimum values of the electromagnetic force stabilize within each cycle, and the pattern of electromagnetic force variation remains consistent.

From Fig. 8, it can be observed that with the continuous increase in the power-on duration within each cycle, both the maximum ($F_{\max}$) and minimum ($F_{\min}$) values of the steady-state electromagnetic force increase. When the power is on for 20ms and off for 180ms within each cycle, the maximum value $F_{\max}$ of the electromagnetic force is still insufficient to overcome the load force. When the power is on for 30ms and off for 170ms within each cycle, the electromagnetic force successfully overcomes the load force to achieve the ejection. However, at this point, due to the armature attraction, there is a nonlinear increase in electromagnetic force. After the zero-voltage natural discharge occurs over 170 milliseconds, the minimum electromagnetic force within the steady-state cycle still exceeds the load force. This means that the actuator cannot be retracted after ejecting.

2) ANALYSIS OF CAPACITY CONTROL CHARACTERISTICS

Fig. 9 illustrates the variation of compressor load, electromagnetic force extremes, and load force extremes with the control parameter energization time $T_{\phi 1}$ under single voltage drive mode. From the results, it can be observed that under the single-voltage drive mode, regardless of the voltage magnitude and the change in energization time, the compressor load can only switch between 100% and 0%. This is because the electromagnetic force undergoes nonlinear changes after the armature is attracted, and before the actuator is fully ejected, the maximum value of the electromagnetic force is less than the minimum value of the load force, preventing the suction valve from opening, resulting in the compressor operating at full load. After the actuator is fully ejected, the

TABLE 2. Configuration of compressor system parameters.

Item	Value	Item	Value
Suction pressure p_s (Kpa)	100	motor speed (rpm)	300
Discharge pressure p_d (Kpa)	250	Unloader spring pre-compression x_0 (mm)	4.5
Valve lift x_{value} (mm)	2	Adiabatic process index k_e	1.4
Crankshaft radius r (mm)	90	Actuator stroke x_δ (mm)	3
Length of connecting rod l (mm)	450	Return spring stiffness K (N/m)	100000
Piston rod radius (mm)	22.5	Piston radius D_{cv} (mm)	125
clearance volume (mm^3)	1.26E+06	offset angle θ_{offset} ($^\circ$)	0

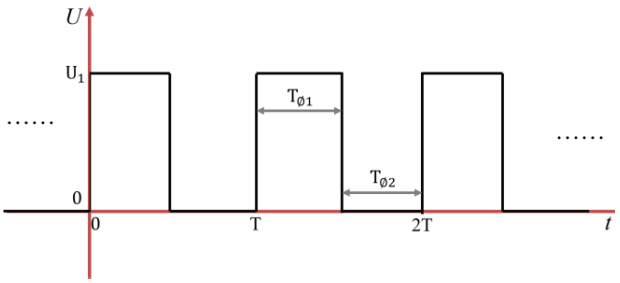

FIGURE 7. Illustration of on/off control parameters in single-voltage mode.

electromagnetic force experiences nonlinear growth, and the minimum value of the electromagnetic force is greater than the maximum value of the load force, preventing the suction valve from closing, and resulting in the compressor operating at zero load.

C. SIMULATION STUDY OF THE POSITIVE AND REVERSE DUAL-VOLTAGE DRIVE MODE

Through the analysis of the previous section, we concluded that the single-voltage on-off drive mode is not suitable for the ECC. To address this issue and improve the descent speed of electromagnetic force after ejection, it is necessary to modify the on-off control mode by replacing the 0 voltage with reverse voltage. This section conducts a study on the driving mode based on positive and reverse voltage excitations. The schematic diagram of the positive and reverse dual-voltage excitation signal is shown in Fig. 10, where $T_{\phi 1}$ represents the excitation time of the positive voltage U_1, $T_{\phi 2}$ represents the excitation time of the reverse voltage U_2, and the total duration of positive and reverse voltage actions still equals one-period length.

At this point, the three expansion coefficients can be obtained as follows using (21):

$$\begin{cases} A_0 = U_1 \cdot \phi_1 + U_2 - U_2 \cdot \phi_1 \\ A_k = \dfrac{\sin(2k\pi\phi_1)}{k.\pi} \cdot (U_1 - U_2) \\ B_k = \dfrac{1 - \cos(2k\pi\phi_1)}{k.\pi} \cdot (U_1 - U_2) \\ \phi_1 = \dfrac{T_{\phi 1}}{T} \end{cases} \tag{31}$$

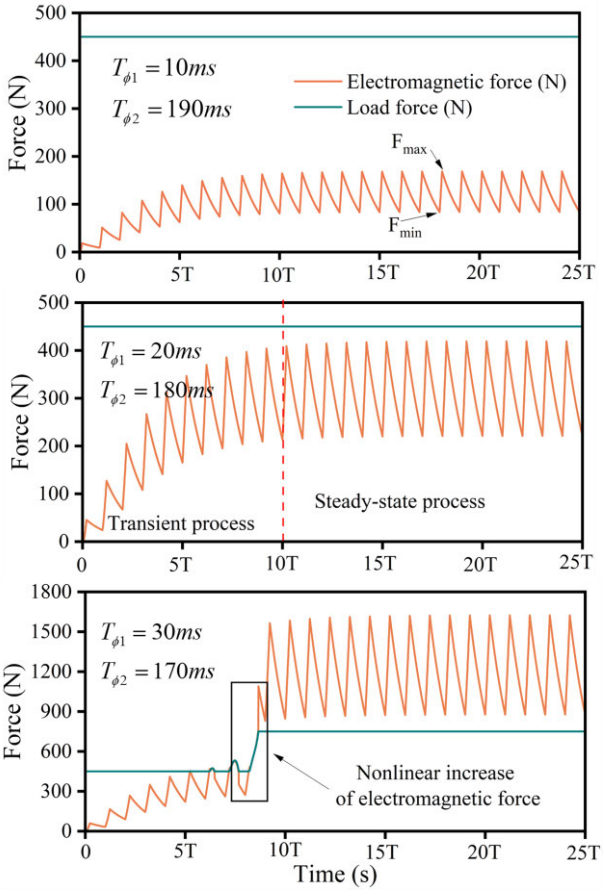

FIGURE 8. Schematic diagram of the response relationship between electromagnetic force and load force over 25 cycles.

Firstly, analyze the relative variation relationship of the extremum values of electromagnetic force and load force within the steady-state cycle under different combinations of positive and reverse voltage magnitudes and excitation time, as shown in Fig. 11.

From the results shown in Figs. 11 (a), (b), and (c), the following conclusions can be drawn:

1) Compared to the results under the single-voltage on-off control mode shown in Figure 10, the introduction of reverse voltage significantly improves the nonlinear

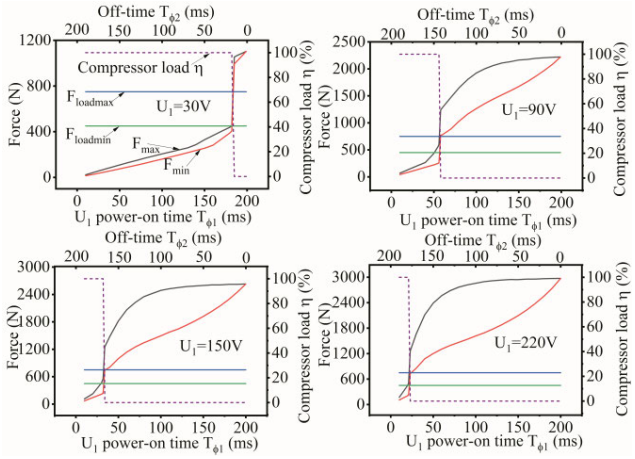

FIGURE 9. Analysis of capacity control characteristics under single voltage drive mode.

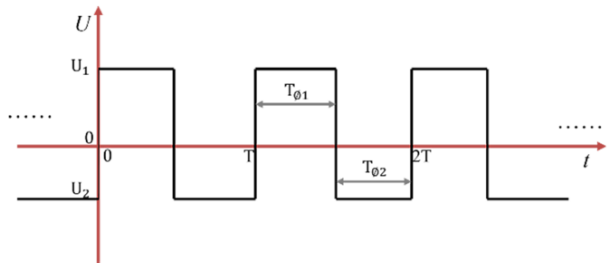

FIGURE 10. Schematic representation of control parameters for positive and reverse dual-voltage excitation.

variation of the electromagnetic force extremum. In each voltage combination, there appears a time region that satisfies the single-cycle response condition, i.e., $F_{\max} \geq F_{load\,\max}$, $F_{\min} \leq F_{load\,\min}$.

2) The electromagnetic actuator exhibits two time regions in a single-cycle response. When the positive voltage magnitude and duration are large, the electromagnetic actuator engages under the positive voltage and disengages under the reverse voltage, defined as the positive engagement response region Δt_p. When the reverse voltage magnitude and duration are large, the electromagnetic actuator engages under the reverse voltage and disengages under the positive voltage, defined as the reverse engagement response region Δt_r.
3) When the positive voltage U_1 is greater than the reverse voltage U_2, the positive engagement response region Δt_p performs well and has a broader range. In this case, the maximum and minimum values of the electromagnetic force ($F_{\max}$ and $F_{\min}$) increase with the increase in the excitation time $T_{\phi1}$. Conversely, when the positive voltage U_1 is less than the reverse voltage U_2, the reverse engagement response region Δt_r performs well and has a broader range. In this scenario, the maximum and minimum values of the electromagnetic force ($F_{\max}$ and $F_{\min}$) increase with the increase in the excitation time $T_{\phi2}$.

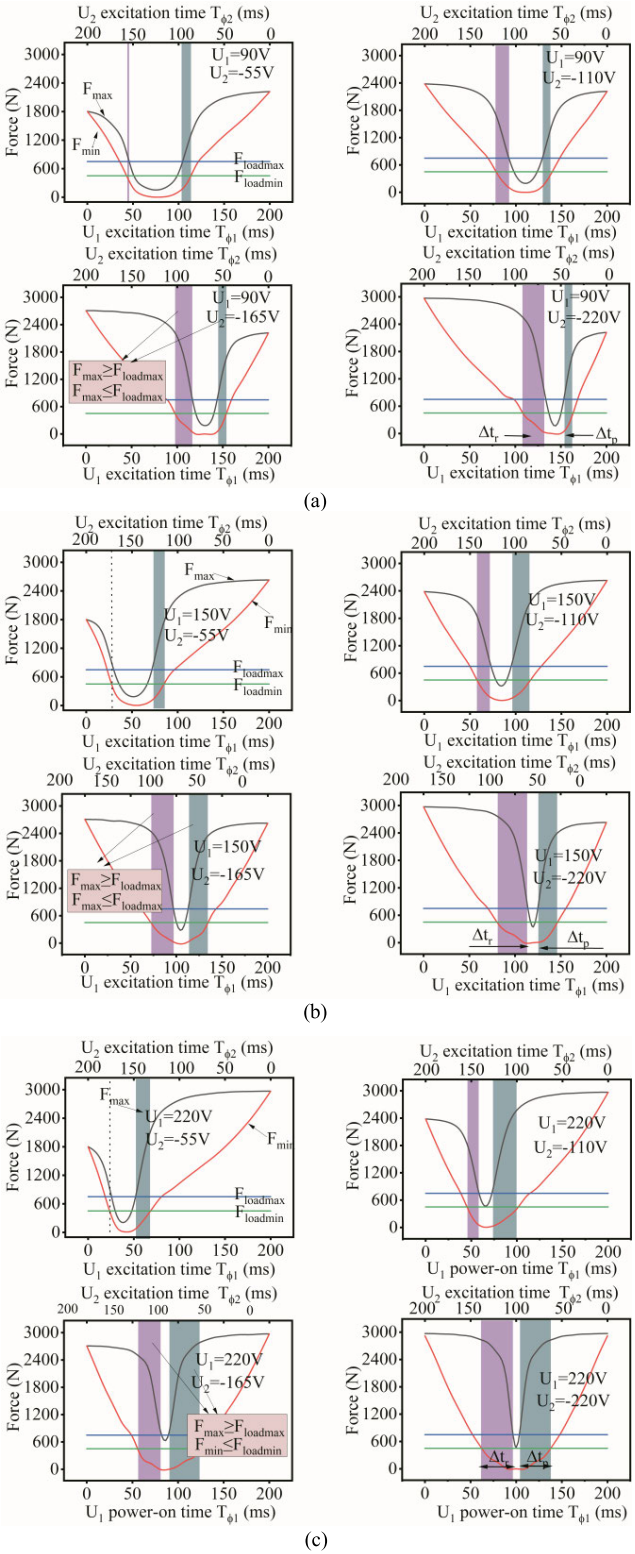

FIGURE 11. Variation patterns of the extremum values of electromagnetic force and load force.

Building upon the aforementioned study, further research was conducted on the variation patterns of thermodynamic parameters, the phase angle θ_{bf}, and the compressor load

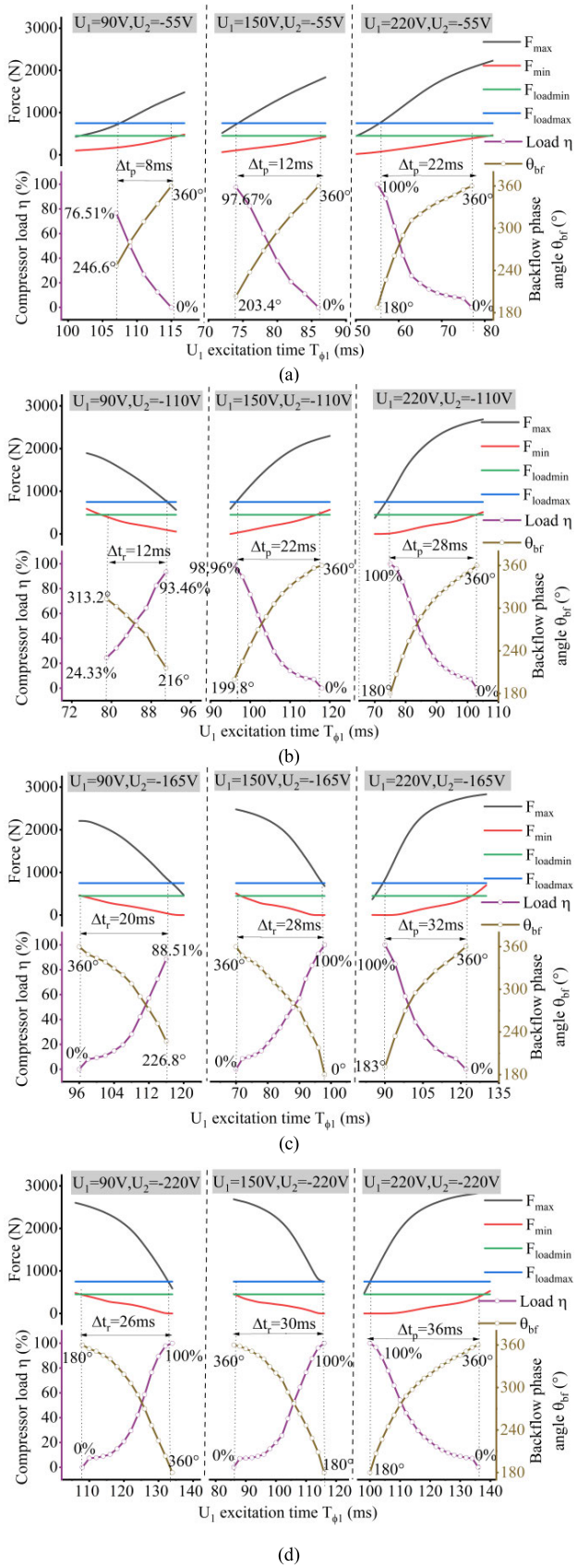

FIGURE 12. Variation patterns of the thermodynamic target parameters under different control parameters.

ratio η to energization time within the single-cycle response region. By selecting the optimal response ranges corresponding to different voltage combinations in Fig. 11, we obtained results through model simulation as illustrated in Fig. 12.

Fig. 12 shows the influence of control parameter variation on capacity control performance under positive and negative dual-voltage drive mode. It can be seen from the diagram that the positive and negative double voltage excitation can effectively improve the response characteristics of the actuator and the capacity control performance of the compressor, it is evident that when the positive voltage surpasses the reverse voltage, within the positive engagement response region, an increase in the on-time of positive voltage and a decrease in the on-time of reverse voltage within a single cycle lead to an increase in the phase angle θ_{bf} and a decrease in the compressor load η. Conversely, when the positive voltage is less than the reverse voltage, the reverse engagement response region performs more effectively. In this scenario, an increase in the on-time of positive voltage and a decrease in the on-time of reverse voltage within a single cycle result in a decrease in the phase angle θ_{bf} and an increase in the compressor load η.

In addition, as the difference between positive and reverse voltages increases, there is a noticeable improvement in the accuracy and range of capacity control for the compressor. However, this also indicates an increase in the power consumption and energy consumption of the electromagnetic actuator. For example, when the positive and reverse excitation voltages for the actuator are 90 V/-55 V, the capacity control range is 0% to 76.51%, with an adjustable time interval of 8 milliseconds. This corresponds to a capacity control accuracy of 9.56% per millisecond. When increasing the magnitude of positive and reverse voltages to the maximum rated voltage, i.e., 220 V/-220 V, the actuator's power consumption reaches its maximum. At this point, the single-cycle response and capacity control performance of the actuator are optimal, with a capacity control range of 0% to 100%, and the maximum adjustable time interval reaching 36 milliseconds. However, the capacity control exhibits a nonlinear variation pattern with energization time. Within the range of 0% to 20% load variation, the corresponding adjustable time is approximately 16 milliseconds, with a capacity control accuracy of approximately 1.25% per millisecond. When the load varies within the range of 100% to 20%, the corresponding adjustable time is approximately 20 milliseconds, with a capacity control accuracy of approximately 4% per millisecond. This indicates that the capacity control accuracy in this range remains challenging to meet the requirements.

D. SENSITIVITY ANALYSIS

Figs. 11 and 12 clearly illustrate the impact of control parameters, such as voltage magnitude and timing, on key objectives like electromagnetic force, reflow termination phase angle, and compressor load. Furthermore, this paper employs the Sobol method [26] for an in-depth sensitivity analysis of these control parameters. The Sobol method, based on the

TABLE 3. Sensitivity index calculation results.

Parameter	Sensitivity index	
	First-order sensitivity index	Total sensitivity index
Positive voltage magnitude	0.0674	0.0108
Negative voltage magnitude	-0.1336	0.0152
Positive voltage stimulation duration	0.3844	0.5233

principle of variance decomposition, is particularly effective in identifying the sensitivity of parameter interactions in highly nonlinear models, and its results exhibit a high degree of robustness and reliability [27]. Since the electromagnetic force and reflow termination phase angle are intermediate variables within the system, while the compressor load is the final output of the system model, this study focuses on analyzing the sensitivity of the load output to these three control parameters. Through this analysis, we can identify the parameters that have the greatest impact on system performance, providing an important reference for the design of the system controller. The ECCS under study can be described by Equation (32), which details the mathematical model of the system's dynamic behavior.

$$\boldsymbol{Y} = f(x) = f(X_1, X_i \ldots X_n) \tag{32}$$

The first-order sensitivity index is calculated as follows:

$$S_i = \frac{\mathrm{Var}(E\left[\boldsymbol{Y} \mid X_i\right])}{\mathrm{Var}(\boldsymbol{Y})} \tag{33}$$

where $E\left[\boldsymbol{Y} \mid X_i\right]$ is the expected value of output $\boldsymbol{Y}$ given the parameter X_i. $Var(\boldsymbol{Y})$ is the variance of output $\boldsymbol{Y}$.

The total effect index is calculated as follows:

$$ST_i = \frac{\mathrm{Var}(E\left[\boldsymbol{Y} \mid \mathrm{all} X_{j \neq i}\right]) - \mathrm{Var}(E\left[\boldsymbol{Y} \mid X_i\right])}{\mathrm{Var}(\boldsymbol{Y})} \tag{34}$$

where $E\left[\boldsymbol{Y} \mid \mathrm{all} X_{j \neq i}\right]$ is the expected value of output $\boldsymbol{Y}$, given all parameters are fixed except for X_i.

The results of the Sobol method sensitivity analysis are shown in Table 3.

The first-order influence index of the positive voltage magnitude is 0.0674, indicating that the positive voltage magnitude has a positive effect on the compressor load, but its impact is relatively minor. The first-order influence index of the negative voltage magnitude is −0.1336, which suggests that the negative voltage magnitude has a negative effect on the compressor load, and its degree of influence is slightly greater than that of the positive voltage magnitude. The first-order influence index of the positive voltage duration is 0.3844, demonstrating that the positive voltage duration has a significant positive impact on the compressor load, and it is the most influential among the three parameters.

The total effect index of the positive voltage magnitude is 0.0108, which means that after considering the interactions of all parameters, the impact of the positive voltage magnitude on the compressor load is relatively minor. The total effect index of the negative voltage magnitude is 0.0152, indicating that the overall impact of the negative voltage magnitude is slightly greater than that of the positive voltage magnitude, but it is still not the most significant influencing factor. The total effect index of the positive voltage duration is 0.5233, demonstrating that after taking into account the interactions of all parameters, the positive voltage duration continues to have the greatest impact on the compressor load.

In summary, the positive voltage duration has the most pronounced impact on the compressor load, regardless of whether it is viewed from the perspective of the first-order or total effect index. The influence of the positive and negative voltage magnitudes is relatively minor, but the absolute value of the first-order influence index for the negative voltage magnitude is greater than that for the positive voltage magnitude, indicating that its impact on the load may be more pronounced. These results suggest that controlling the load by selecting the positive voltage duration can achieve better outcomes.

V. DESIGN OF CAPACITY CONTROL PROCEDURE BASED ON FDTSVD METHOD

In an in-depth analysis of the interaction between the dynamic behavior of actuators and the suction valve of compressors, it has been recognized that the duration and timing of the excitation signal have a significant effect on the dynamic response of the actuator and the capacity control effect. Therefore, developing effective control strategies to precisely manage these two key variables is particularly critical. This study innovatively proposes a load regulation method named FDTSVD load regulation method, which integrates three core concepts: Fixed Duration (FD), Variable Duration (VD), and Timing Shift (TS).

The concepts of FD and VD have been widely adopted in the fields of psychology and behavioral science [28], [29], [30] to explore the specific impact of stimulus duration on behavioral responses. This study draws on the research achievements of these fields and deeply explores the impact of the duration of the excitation signal on the dynamic behavior of the actuator through these two methods. In addition, this study innovatively introduces the concept of timing shift [31] and combines it with fixed duration to adjust the timing of the action of the excitation signal, thereby further optimizing the dynamic response of the actuator and the capacity control effect of the compressor.

As shown in Fig. 13(a), as the positive time sequentially changes from T_{11} to T_{12} and T_{13} at equal intervals, the actuator's ejection phase angle continuously decreases, and the retract phase angle increases. The pressure variation in the compressor's volumetric chamber also changes with the backflow phase angle. This regulation is called VD. It should be noted that when the actuator's ejection phase varies within the range of 0 to 180 degrees, it has no significant impact on the capacity control function. On the contrary, premature ejection increases the energy consumption of the actuator.

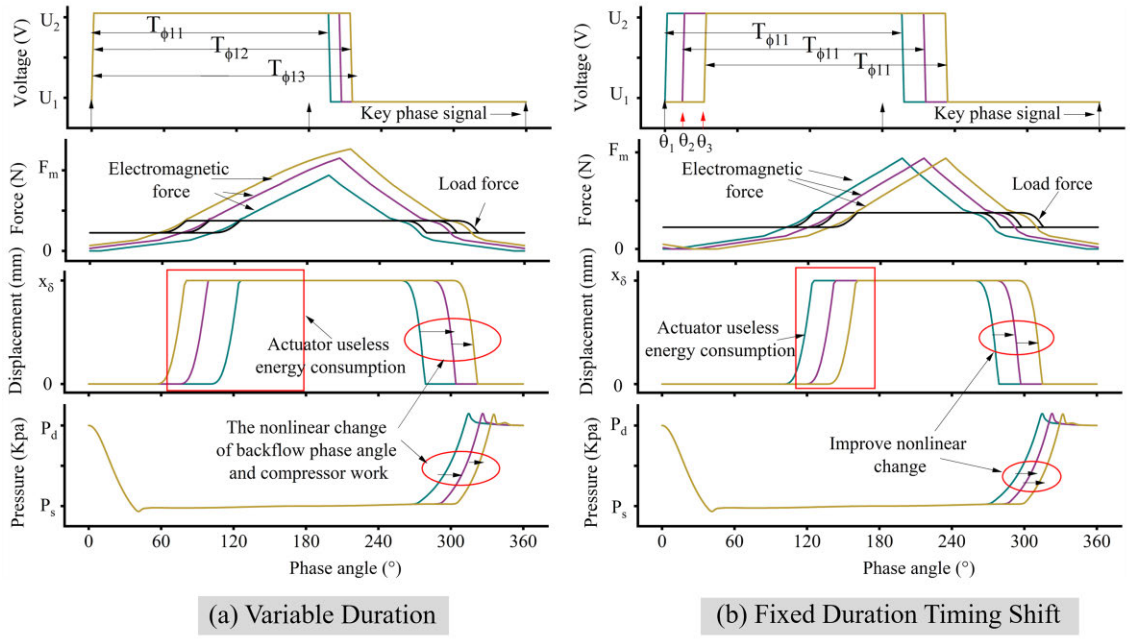

FIGURE 13. FDTSVD method schematic diagram.

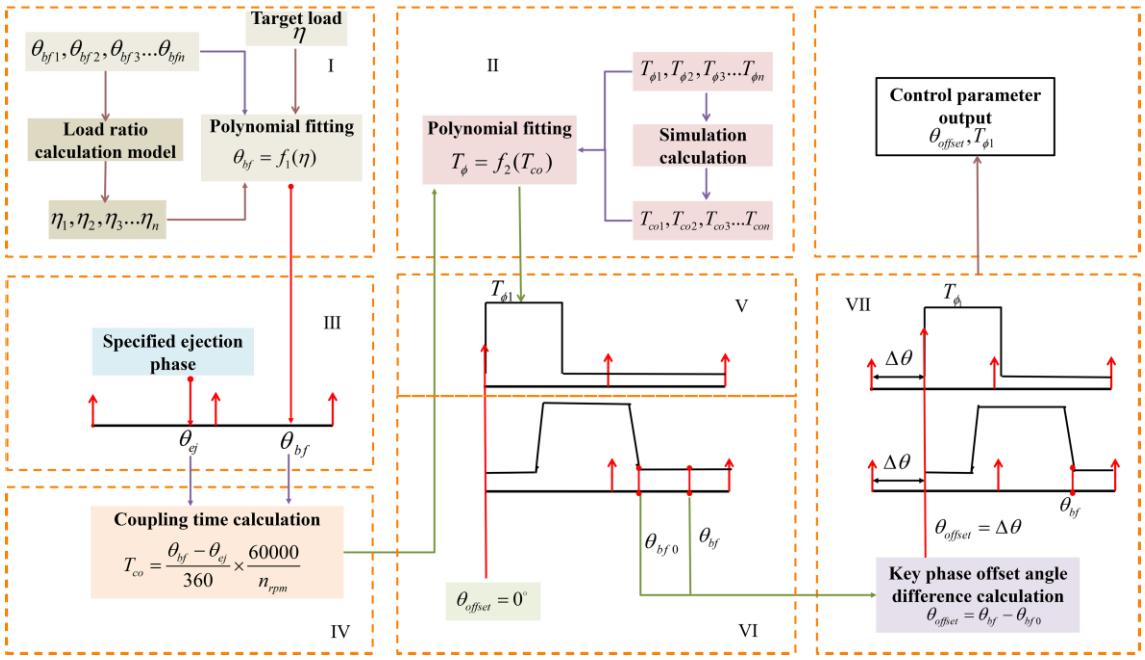

FIGURE 14. Capacity control strategy flowchart.

Therefore, by changing the timing of excitation for the control signal, while ensuring that the duration of the actuator's ejection remains unchanged, linearly altering the ejection and retraction positions of the actuator becomes a key measure to improve the linearity of capacity control and reduce the energy consumption of the actuator, this regulation is called Fixed Duration Timing Shift (FDTS), as shown in Fig. 13(b).

While maintaining the duration of the positive electrical excitation ($T_{\phi 1}$) unchanged, the timing of the excitation voltage is changed in equal intervals, applied successively after the key phase signals θ_1, θ_2, and θ_3. It can be observed that the ejection and retraction positions of the actuating mechanism linearly shift backward in sequence. Moreover, the ejection holding phase of the actuator before 180° is significantly

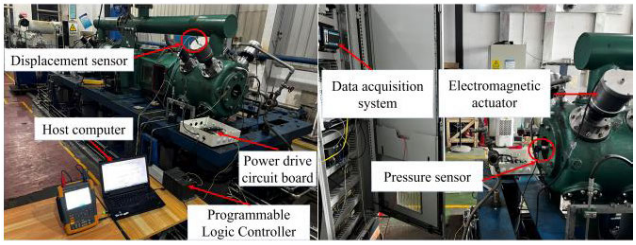

FIGURE 15. Reciprocating compressor electromagnetic capacity control experimental rig.

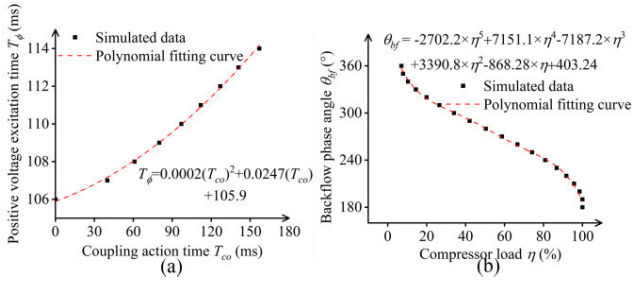

FIGURE 16. Polynomial fitting curve.

reduced compared to the adjustment method of changing the voltage time. This indicates that a wider range of capacity control can be achieved with lower energy consumption of the actuator.

This article comprehensively employs the concepts of FDTSVD. It utilizes time-shift scheduling to alter the timing of actuator excitation signals, and variable time scaling to modify the duration of these signals. Consequently, the compressor capacity control procedure is designed. The flow chart of the control algorithm is shown in Fig. 14, and the pseudo code is as follows:

1) Based on the load ratio calculation model established in Section III, the variation in compressor load (η) with respect to the backflow termination phase angle (θ_{bf}) is determined. Utilizing this data, a reverse polynomial fitting is performed to derive the function $\theta_{bf} = f_1(\eta)$, which represents the relationship between the backflow termination phase angle and load variations.
2) The variation of the coupling action time (T_{co}) of the actuator and the suction valve with the control parameter positive energization time ($T_{\phi 1}$) is obtained by simulation. Based on this data, a transformation function $T_{\phi 1} = f_2(T_{co})$ was derived using polynomial fitting.
3) Specify the initial coupling phase angle, θ_{ej}, between the actuator and the suction valve. Using the target load, calculate the ideal backflow termination phase angle, θ_{bf}, based on the fitting function from Step (1).
4) By using the ideal backflow termination phase angle, θ_{bf}, and the specified initial coupling phase angle, θ_{ej}, calculate the coupling action time, $T_{co} = (\theta_{bf} - \theta_{ej})/360 \times 60000/n_{rpm}$, between the actuator and the suction valve.

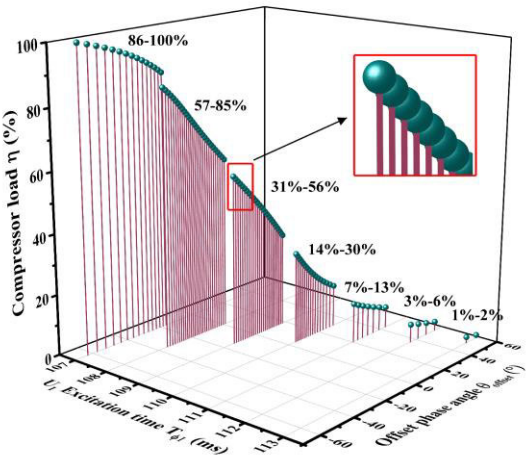

FIGURE 17. Calculation results of control parameters under different compressor loads.

5) Based on the coupling action time T_{co} from Step (4) and the fitting function $T_{\phi 1} = f_2(T_{co})$ from Step (2), determine the positive energization time $T_{\phi 1}$.
6) Input the solved actuator control parameters $T_{\phi 1}$ into the established working model, setting $\theta_{offset} = 0^\circ$. This process yields the actual backflow termination phase angle of the compressor θ_{bf0} under a keyless phase offset scenario.
7) Based on the ideal backflow termination phase angle θ_{bf} calculated for the target load, and the actual backflow termination phase angle θ_{bf0} obtained without key phase offset, solve to determine the required key phase offset $\theta_{offset} = \theta_{bf} - \theta_{bf0}$.

Based on the aforementioned steps, it is possible to obtain a combination of control parameters for the actuator that minimizes energy consumption under any load condition. This approach not only enhances the precision of capacity control but also reduces the energy consumption of the actuator itself.

VI. EXPERIMENTAL VALIDATION

As illustrated in Fig. 15, an experimental rig was set up to validate the accuracy of the developed model and the effectiveness of the proposed capacity control method. The compressor used in the laboratory test rig is a DW-12/2 model. The setup of relevant system parameters is consistent with Table 2, and the settings for the electromagnetic actuator align with those in Table 1. The data acquisition system is capable of real-time collection of sensor signals for displacement, phase, current, and pressure. It achieves synchronous continuous acquisition across 32 channels at a sampling frequency of 25.6 kHz and converts sensor measurements for transmission to a PLC. The PLC, a Siemens S7-300 model, is responsible for real-time calculation of valve opening signals and actuator energization times (both forward and reverse), based on collected crankshaft key phase signals and given load values. These control parameters are

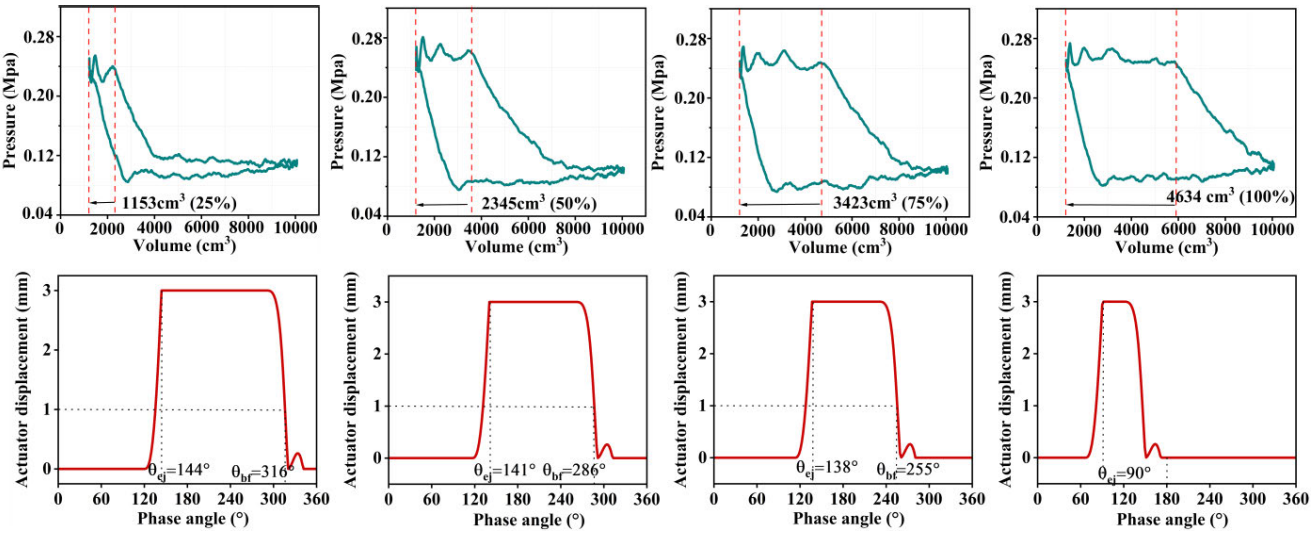

FIGURE 18. Dynamic pressure and actuator displacement response under different loads.

TABLE 4. Calculation of intermediate parameters under different load conditions.

Intermediate parameters	Discharge load			
	25%	50%	75%	100%
Ideal backflow termination phase angle θ_{bf} (°)	311	281	249	180
Coupling action time between the actuator and the suction valve T_{co} (ms)	89	72.7	55	16.6
Positive voltage excitation time $T_{\phi 1}$ (ms)	110	109	108	107
Actual backflow termination phase θ_{bf0} (°)	301	286	270	250
Key phase offset angle θ_{offset} (°)	10	-5	-21	-70

TABLE 5. The change of thermodynamic performance parameters under different loads.

Thermodynamic parameter	Discharge load			
	25%	50%	75%	100%
Discharge pressure (Kpa)	240	253	244	247
Indicator work (J)	175.2	338.6	463.4	593.6
Compression energy efficiency (cm³/J)	6.58	6.94	7.41	7.81
Energy saving efficiency (%)	70.5	43	21.9	0

then transmitted to a field drive board, which converts them into excitation voltages for the actuator.

As indicated in the simulation results of Section IV, when the actuator operates at the minimum response power voltage of 90 V/-55 V, the capacity control range is 0%-76.51%, with a capacity control precision of 9.56% per millisecond. This paper focuses on the 90 V/-55 V voltage excitation as an example. Through the model simulation, the variation law of the coupling time between the electromagnetic actuator and the suction valve with the forward voltage excitation time is determined. This relationship $T_{\phi} - T_{co}$ was derived through a second-order polynomial fitting [32], [33], as shown in Fig. 16(a). Furthermore, using the compressor capacity control working model established in Section III, the variation in compressor load under different backflow termination phase angles was obtained. This was fitted with a reverse fifth-order polynomial to establish the $\theta_{bf} - \eta$ function relationship, as illustrated in Fig. 16(b):

It can be seen from the analysis of Fig. 13 that when the actuator is ejected too earlier than 180°, the ejecting holding time of the actuator is too long, which will increase the energy consumption of the actuator itself. Conversely, activation too close to 180° can lead to delayed response errors during the valve closure process, increasing the risk of collisions between the actuator and the valve. Therefore, this paper stipulates that the actuator's ejection phase angle, θ_{ej}, should be fixed around 150°. Building on these steps, the algorithm proposed in Section V was used to determine control parameters for various loads, as shown in Fig. 17.

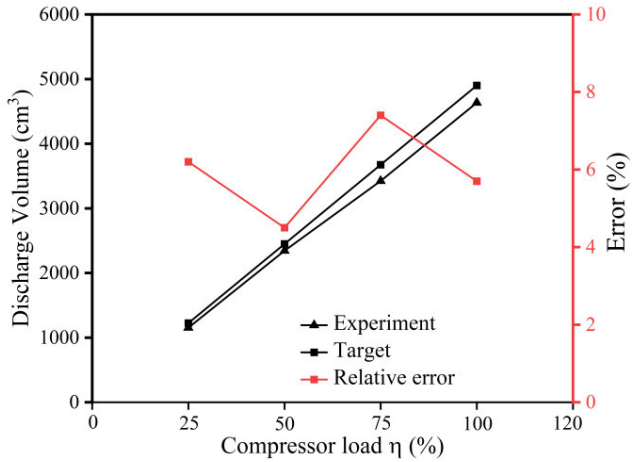

FIGURE 19. The relative error in discharge volume.

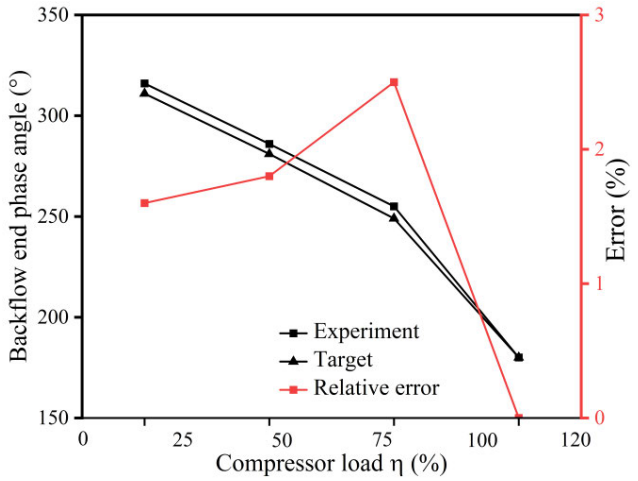

FIGURE 20. The relative error in backflow termination phase angle.

Further, to verify the effect of the control, load values of 25%, 50%, 75%, and 100% were selected for testing. The backflow termination phase angle θ_{bf}, coupling action time T_{co}, positive voltage energization time $T_{\phi 1}$, and key phase offset angle θ_{offset} were calculated for these four different load conditions, as shown in Table 3.

Based on the control parameters derived from Table 4, experiments were conducted to obtain the dynamic pressure in the compressor's volume chamber and the actuator's displacement response under different load conditions, as depicted in Fig. 18.

Based on the experimental results obtained in Fig. 18, the effect of electromagnetic capacity control is further analyzed in detail through thermodynamic performance parameters such as discharge pressure, indicator work, compression energy efficiency, and energy saving efficiency. The indicator work W is based on the Matlab software and obtained by the polyarea function algorithm, that is:

$$W = \text{Polyarea}(\boldsymbol{V}, \boldsymbol{P}) \tag{35}$$

The compression energy efficiency E_η is defined as the ratio of the compressor's single-cycle discharge volume to the indicator work consumption, which characterizes the target pressure gas volume that the compressor can discharge per unit energy consumption.

$$E_\eta = \frac{V_d}{W} \tag{36}$$

The energy saving efficiency E_S is defined as the ratio of the indicated work saved under different discharge loads of the compressor relative to full load operation:

$$E_S = \frac{W_{100\%} - W_\eta}{W_{100\%}} \times 100\% \tag{37}$$

Through data post-processing, other thermodynamic parameters of the compressor under different discharge loads are shown in Table 4. It can be seen from Table 4 that the ECCS has a significant energy-saving effect and reliable working performance. When the exhaust load is 25%, the single cycle indication function consumption decreases from 593.6 J of 100 % load to 175.2 J, and the energy saving efficiency is as high as nearly 70.5%. The discharge pressure error under different loads is stable in the range of ±10 Kpa. It is worth noting that when the load becomes lower, the compression energy efficiency is also reduced. When the load decreases from 100% to 25%, the gas volume under the target pressure that can be discharged under unit energy consumption decreases from 7.81 cm^3 to 6.58 cm^3. Therefore, how to optimize the design of system parameters to improve the compression energy efficiency under different loads has become the focus of future research.

From Figs. 19 and 20, it can be observed that the proposed load control method performs well under different load conditions. The accuracy of control is determined by the relative error between the actual value and the target [34]. The relative error between the experimental exhaust volume and the target value under all loads does not exceed 7.5%, and the errors in the backflow termination phase angle do not exceed 3%, which are primarily influenced by system deviations such as mechanical and control variances. This validates the reliability of the established working model and the effectiveness of the control procedure.

Although the designed ECCS can significantly enhance the operational efficiency of reciprocating compressors, special attention must be given to the following potential challenges when implementing ECCS on existing compressors, along with corresponding resolution strategies:

1) Intake valve modification issue: To accommodate the installation of the ECCS actuator, the original intake valve requires modification. The following measures are recommended:
   - Conduct a thorough analysis of the valve structure and performance to determine the necessity and feasibility of the modification.
   - Design and manufacture specialized adapters or conversion parts to ensure that the ECCS actuator

TABLE 6. The main components of the ECCS and their corresponding carbon emission coefficients.

Component	Quantity	Carbon emission factor	Boundary	Cost (yuan)
Electromagnet	12 piece	332.32 $kgCO_2$-eq/piece	production to disposal	5000
Unloader	12×3 kg	2.3 $kgCO_2$-eq/kg	production to disposal	3000
Control system hardware	1 set	2090 $kgCO_2$-eq/set	production to use	20000
Cable	1000 m	0.25 $kgCO_2$-eq/m	production to use	13
Computer	1 piece	738 $kgCO_2$-eq/piece	production to use	7000
Server	1 piece	294.8 $kgCO_2$-eq/piece	production to use	20950

TABLE 7. The main components of the HCCS and their corresponding carbon emission coefficients.

Component	Quantity	Carbon emission factor	Boundary	Cost (yuan)
Hydraulic cylinder	12×7.5kg	2.3 $kgCO_2$-eq/kg	production to disposal	5000
Unloader	12×3kg	2.3 $kgCO_2$-eq/kg	production to disposal	3000
Control system hardware	1 set	2090 $kgCO_2$-eq/ set	production to use	20000
Cable	1000 m	0.25 $kgCO_2$-eq/m	production to use	13
Computer	1 piece	738 $kgCO_2$-eq/ piece	production to use	7000
Server	1 piece	294.8 $kgCO_2$-eq/ piece	production to use	20950
Hydraulic oil	175 kg	5.26 $kgCO_2$-eq/ kg	production to disposal	2300
Petrol station	300 kg	18.30 $kgCO_2$-eq/kg	production to use	80000
Hydraulic hard	100 kg	2.3 $kgCO_2$-eq/kg	production to use	4000
Hydraulic hose	25 kg	2.73 $kgCO_2$-eq/kg	production to use	3000
Electric motor	1 piece	332.32 $kgCO_2$-eq/ piece	production to disposal	5000

TABLE 8. Comparison of total carbon emissions and costs between two systems.

System	Total carbon emissions	Total cost (ten thousand yuan)
ECCS	7443.44 $kgCO_2$	15.695
HCCS	10578.67 $kgCO_2$	22.075

is compatible with the existing intake valve installation.

- During the modification process, ensure that the sealing performance and durability of the valve are not affected, while optimizing the valve's flow characteristics to enhance overall performance.

2) Dynamic characteristics of the electromagnetic actuator: The electromagnetic actuator in the ECCS is sensitive to air gap variations, hence the following suggestions are made:

- Optimize the structure of the electromagnetic actuator during the design phase to reduce sensitivity to changes in the air gap.
- Use high-precision measuring tools and methods during the installation process to strictly control installation errors and ensure the air gap is within the designed range.
- Train operators to fully understand the working principles and maintenance requirements of the electromagnetic actuator, reducing errors caused by human factors.

With these meticulous considerations and thoughtful measures, it is possible to effectively address the challenges that may be encountered when applying ECCS to existing reciprocating compressors, ensuring the smooth implementation and efficient operation of the system.

VII. ENVIRONMENTAL AND ECONOMIC ANALYSIS

This article employs the life cycle analysis method [35], [36] and compares it with the HCCS described in the literature [13], in order to analyze the environmental and economic impacts of transitioning from HCCS to ECCS. The study selects the production of a set of CCS and ensures stable operation for one year (i.e., 8000 hours) as the functional unit to analyze the impact of CCS on the environment and economy. In the environmental evaluation, carbon emissions are chosen as a key indicator to quantify the potential environmental impact of the system.

Table 6 and Table 7 provide a detailed list of the main components and their required quantities within the functional unit of the two systems. Over a one-year (8000-hour) operating period, there are significant differences in the degree of consumption of different components, leading to

TABLE 9. Energy saving and carbon emission calculations under different operating loads.

Unit load	Energy-saving load	Saved indicated power (kW)	Annual electricity cost savings (ten thousand yuan)	Reduce carbon emissions (kg CO_2)
100%	0	0 kW	0	0
80%	20%	119 kW	48	553112
60%	40%	239 kW	96	1110872
37% (Common operating conditions)	63%	376 kW	150	1747648
20%	80%	478 kW	191	2221744

corresponding changes in the boundaries of analysis. For instance, moving parts in the CCS, such as electromagnetic actuators and hydraulic actuators, have an analysis boundary that covers the entire lifecycle from production (cradle) to disposal (grave) due to the need for regular replacement. In contrast, other components that are less prone to damage can operate for a long time, so their analysis boundary is limited to the production to use phase (from cradle to gate). To obtain the carbon emission factors corresponding to each component, the study refers to the ''China Product Life Cycle Greenhouse Gas Emission Coefficient Library,'' a resource that provides key data for assessing the environmental impact of each component throughout its entire lifecycle.

Taking the operating data of the hydrogen compressor in the exhaust gas workshop of a certain photovoltaic electronics company as an example, this article conducts an in-depth analysis of the carbon emissions and economic performance during the operation of the CCS. The compressor is driven by an electric motor with a rated power of 1250 kW. Under specific conditions of an intake pressure of 0.591 MPa and an exhaust pressure of 1.385 MPa, the shaft power of the unit at rated full load operation is 854 kW. The indicated power of the gas, which is the actual power consumed by the gas, is approximately 70% of the shaft power, resulting in an indicated power of about 597 kW.

Currently, the average operating load of the unit is 37%, and the excess gas volume is regulated through a recirculation valve. However, on average, 63% of the excess gas is compressed repeatedly, leading to significant energy waste. After the installation of the CCS, the recirculation valve can be completely closed, thus saving the energy required to compress 63% of the excess gas.

Further, with the addition of CCS, the energy-saving effects under different loads are remarkable, and the specific energy-saving data are presented in Table 9. This improvement not only enhances the system's energy efficiency but also helps to reduce carbon emissions, achieving optimization on both economic and environmental fronts.

The formula for calculating annual electricity cost savings is as follows:

Annual electricity cost savings = Saved indicated power × Operating hours × Unit price (industrial electricity at 0.5 yuan/kWh)

The formula for calculating the reduction in carbon emissions during operation is as follows:

Reduce carbon emissions = Saved indicated power × Operating hours × Average grid emission factor (0.581 $kgCO_2$/kWh)

Through the comparative analysis of Tables 6-8, it is evident that the ECCS has made significant progress in simplifying the system components compared to the HCCS. This simplification is not only reflected in the design but also in the total carbon emissions of a single set of the system, which has been significantly reduced from 10263.17 $kgCO_2$ to 7443.44 $kgCO_2$, while the cost has also been reduced from 220750 yuan to 156950 yuan. Such improvements have brought significant enhancements in both environmental impact and economic viability.

The data in Table 9 further reveal the remarkable effects of a single set of CCS in saving electricity cost and reducing carbon emissions over an 8000-hour operating period in one year. Especially under the common operating condition of 37% load, the energy-saving rate reaches 63%. Under this load condition, the annual electricity cost savings can reach 1.5 million yuan, while reducing carbon emissions by 1747648 $kgCO_2$. This indicates that the system can achieve positive returns in both economic and environmental benefits within just one year, making a positive contribution to promoting sustainable development.

VIII. CONCLUSION

In this paper, the capacity control working principle model of the coupling control mode of the reciprocating compressor actuator and the suction valve under synchronous frequency with asynchronous actuation is established. The model highlights the complexity of electromagnetic capacity control and provides information for more effective system design. Based on the model, the response characteristics of the electromagnetic actuator and the load regulation characteristics of the compressor under different driving modes and control parameters are studied.

Our research indicates that single-voltage drive modes are ineffective due to self-inductance and armature attraction. In contrast, dual-voltage drive modes enhance actuator responsiveness, improving capacity control. We found that actuators achieve optimal load control at maximum power, enabling a control range of 0% to 100% with a 36-millisecond

adjustment interval. However, precision challenges arise at loads between 100% and 20%.

To overcome these limitations, we selected the optimal control parameters through sensitivity analysis and designed a load control program based on simulation data and the FDTSVD method. The results demonstrate that the actuator achieves step-less capacity control from 0% to 100% at the minimum response power voltage. The accuracy of the adjustment effect was verified under 25%, 50%, 75%, and 100% load conditions. Under each load condition, the relative error between the experimental exhaust volume and the target value under all loads does not exceed 7.5%, and the error in the backflow phase angle was no more than 3%, at the same time, the ECCS has remarkable energy saving effect, stable and reliable operation. When the exhaust load is 25%, the single cycle indication function consumption decreases from 593.6 J of 100% load to 175.2 J, and the energy saving efficiency is as high as nearly 70.5%. The discharge pressure error is stable in the range of ± 10 Kpa under different loads, confirming the effectiveness of the method and the accuracy of the model.

At the same time, environmental and economic analyses indicate that the application of the ECCS system has reduced carbon emissions by 2819.73 $kgCO_2$ compared to the traditional HCCS, reduced costs by 63.8 thousand yuan, and can achieve a positive return on environmental and economic benefits within one year, demonstrating good practical value.

REFERENCES

[1] A. S. Gupta, P. N. N. Thakare, and D. V. S. Gorantiwar, "Analysis of reciprocating compressor valve," *Int. J. Res. Appl. Sci. Eng. Technol.*, vol. 11, no. 3, pp. 1619–1625, Mar. 2023, doi: 10.22214/ijraset.2023.49753.

[2] C. Aprea and C. Renno, "Experimental model of a variable capacity compressor," *Int. J. Energy Res.*, vol. 33, no. 1, pp. 29–37, Jan. 2009, doi: 10.1002/er.1468.

[3] Ö. Kizilkan, "Thermodynamic analysis of variable speed refrigeration system using artificial neural networks," *Exp. Syst. Appl.*, vol. 38, no. 9, pp. 11686–11692, Sep. 2011, doi: 10.1016/j.eswa.2011.03.052.

[4] L. Wang, G. B. Liu, Y. Y. Zhao, and L. L. Li, "Performance comparison of capacity control methods for reciprocating compressors," *IOP Conf. Ser., Mater. Sci. Eng.*, vol. 90, no. 1, Jul. 2015, Art. no. 012029, doi: 10.1088/1757-899X/90/1/012029.

[5] A. A. T. Maia, R. N. N. Koury, and L. Machado, "Development of a control algorithm employing data generated by a white box mathematical model," *Appl. Thermal Eng.*, vol. 54, no. 1, pp. 120–130, May 2013, doi: 10.1016/j.applthermaleng.2013.01.031.

[6] M. Yaqub and S. M. Zubair, "Capacity control for refrigeration and air-conditioning systems: A comparative study," *J. Energy Resour. Technol.*, vol. 123, no. 1, pp. 92–99, Mar. 2001, doi: 10.1115/1.1349117.

[7] T. Bin, Z. Yuanyang, L. Liansheng, L. Guangbin, W. Le, Y. Qichao, X. Haiping, Z. Feng, and M. Wenhui, "Thermal performance analysis of reciprocating compressor with stepless capacity control system," *Appl. Thermal Eng.*, vol. 54, no. 2, pp. 380–386, May 2013, doi: 10.1016/j.applthermaleng.2013.01.036.

[8] W. Hong, J. Jin, R. Wu, and B. Zhang, "Theoretical analysis and realization of stepless capacity regulation for reciprocating compressors," *Proc. Inst. Mech. Eng., E, J. Process Mech. Eng.*, vol. 223, no. 4, pp. 205–213, Nov. 2009, doi: 10.1243/09544089jpme283.

[9] G. Liu, Y. Zhao, B. Tang, and L. Li, "Dynamic performance of suction valve in stepless capacity regulation system for large-scale reciprocating compressor," *Appl. Thermal Eng.*, vol. 96, pp. 167–177, Mar. 2016, doi: 10.1016/j.applthermaleng.2015.11.055.

[10] Q. Xu and W. Hong, "Dynamic performance of reciprocating compressor with capacity regulation system," *Proc. Inst. Mech. Eng., E, J. Process Mech. Eng.*, vol. 233, no. 3, pp. 526–535, Jun. 2019, doi: 10.1177/0954408918772628.

[11] Y. Wang, Z. Jiang, J. Zhang, C. Zhou, and W. Liu, "Performance analysis and optimization of reciprocating compressor with stepless capacity control system under variable load conditions," *Int. J. Refrig.*, vol. 94, pp. 174–185, Oct. 2018, doi: 10.1016/j.ijrefrig.2018.07.013.

[12] L. Yang, X. Jia, H. Qi, J. Feng, X. Peng, and Z. Wang, "Fast algorithm for calculating the pressure pulsation in a reciprocating compressor system with stepless capacity regulation," *Proc. Inst. Mech. Eng., E, J. Process Mech. Eng.*, vol. 233, no. 6, pp. 1280–1291, Dec. 2019, doi: 10.1177/0954408919866602.

[13] X. Sun, J. Zhang, Y. Wang, J. Wang, and Z. Qi, "Optimization of capacity control of reciprocating compressor using multi-system coupling model," *Appl. Thermal Eng.*, vol. 195, Aug. 2021, Art. no. 117175, doi: 10.1016/j.applthermaleng.2021.117175.

[14] P. Naseradinmousavi and C. Nataraj, "Nonlinear mathematical modeling of butterfly valves driven by solenoid actuators," *Appl. Math. Model.*, vol. 35, no. 5, pp. 2324–2335, May 2011, doi: 10.1016/j.apm.2010.11.036.

[15] X. Yuan, S. Shi, C. Wang, L. Wei, C. Luo, and J. Chen, "Dynamic modeling method for an electro-hydraulic proportional valve coupled mechanical–electrical-electromagnetic-fluid subsystems," *J. Magn. Magn. Mater.*, vol. 587, Dec. 2023, Art. no. 171312, doi: 10.1016/j.jmmm.2023.171312.

[16] B. A. Paden, S. T. Snyder, B. E. Paden, and M. R. Ricci, "Modeling and control of an electromagnetic variable valve actuation system," *IEEE/ASME Trans. Mechatronics*, vol. 20, no. 6, pp. 2654–2665, Dec. 2015, doi: 10.1109/TMECH.2015.2389112.

[17] S. Wu, X. Zhao, C. Li, Z. Jiao, and F. Qu, "Multiobjective optimization of a hollow plunger type solenoid for high speed on/off valve," *IEEE Trans. Ind. Electron.*, vol. 65, no. 4, pp. 3115–3124, Apr. 2018, doi: 10.1109/TIE.2017.2756578.

[18] W. Chen, J. Bai, G. Wang, N. Xie, L. Ma, Y. Wang, T. Zhang, and X. Xue, "First and second law analysis and operational mode optimization of the compression process for an advanced adiabatic compressed air energy storage based on the established comprehensive dynamic model," *Energy*, vol. 263, Jan. 2023, Art. no. 125882, doi: 10.1016/j.energy.2022.125882.

[19] M. C. Kulan and N. J. Baker, "Fast analytical force estimation in active magnetic bearings using a magnetic equivalent circuit model," in *Proc. IEEE Int. Electric Mach. Drives Conf. (IEMDC)*, May 2023, pp. 1–7, doi: 10.1109/iemdc55163.2023.10239031.

[20] A. Fan, S. Chang, and H. Chen, "Back-stepping sliding mode control for an electromagnetic valve actuator," *China Mech. Eng.*, vol. 31, no. 3, p. 274, Feb. 2020.

[21] Q. Zhong, B. Zhang, H. C. Hong, and H. Y. Yang, "Three power sources excitation control strategy of high speed on/off valve based on current feedback," *J. Zhejiang Univ.*, vol. 52, pp. 8–15, Jan. 2018, doi: 10.3785/j.issn.1008-973X.2018.01.002.

[22] U. Javaid and D. Dujic, "Arbitrary order generalized state space average modeling of switching converters," in *Proc. IEEE Energy Convers. Congr. Expo. (ECCE)*, Sep. 2015, pp. 6399–6406, doi: 10.1109/ECCE.2015.7310556.

[23] R. F. Q. Magossi, L. J. Elias, F. A. Faria, R. Q. Machado, and V. A. Oliveira, "An *n*-PWM DC–DC converter modeling: Switched systems meets Fourier series," *IEEE Trans. Ind. Electron.*, vol. 69, no. 4, pp. 3255–3265, Apr. 2022, doi: 10.1109/TIE.2021.3071702.

[24] D. Zhao, J. Zhang, L. Dong, Y. Peng, and Y. Wang, "Analysis of dynamic characteristics and adaptive robust control of electromagnetic actuators under variable working conditions," *Arabian J. Sci. Eng.*, vol. 49, pp. 1–19, Mar. 2024, doi: 10.1007/s13369-024-08856-3.

[25] Z. Qi, H. E. Xianjian, L. I. Yanbiao, Z. Bin, Y. Huayong, and C. Bo, "Research on control algorithm for high-speed on/off valves that adaptive to supply pressure changes," *J. Mech. Eng.*, vol. 57, no. 6, pp. 224–235, Mar. 2021, doi: 10.3901/JME.2021.06.224.

[26] Z. Wang, M. Li, F. Ren, B. Ma, H. Yang, and Y. Zhu, "Sobol sensitivity analysis and multi-objective optimization of manifold microchannel heat sink considering entropy generation minimization," *Int. J. Heat Mass Transf.*, vol. 208, Jul. 2023, Art. no. 124046, doi: 10.1016/j.ijheatmasstransfer.2023.124046.

[27] I. M. Sobol, "Global sensitivity indices for nonlinear mathematical models and their Monte Carlo estimates," *Math. Comput. Simul.*, vol. 55, nos. 1–3, pp. 271–280, Feb. 2001, doi: 10.1016/s0378-4754(00)00270-6.

[28] C. Bonardi, E. Mondragón, B. Brilot, and D. J. Jennings, "Overshadowing by fixed- and variable-duration stimuli," *Quart. J. Experim. Psychol.*, vol. 68, no. 3, pp. 523–542, Mar. 2015, doi: 10.1080/17470218.2014.960875.
[29] A. Derenne, "Schedules of reinforcement," in *Encyclopedia of Animal Cognition and Behavior*, J. Vonk and T. K. Shackelford, Eds., Cham, Switzerland: Springer, 2022, pp. 6248–6258.
[30] D. García-Gallardo, F. Aguilar Guevara, C. Canales, S. Moreno, and C. Carpio, "Effects of variable durations of food availability on interval time-place learning with pigeons Columba Livia," *Behavioural Processes*, vol. 179, Oct. 2020, Art. no. 104192, doi: 10.1016/j.beproc.2020.104192.
[31] S. T. P. Purayil, S. A. B. Al-Omari, and E. Elnajjar, "Experimental investigation of spark timing on extension of hydrogen knock limit and performance of a hydrogen-gasoline dual-fuel engine," *Int. J. Hydrogen Energy*, vol. 49, pp. 910–922, Jan. 2024, doi: 10.1016/j.ijhydene.2023.09.139.
[32] M. Bianchi, L. Branchini, A. De Pascale, F. Melino, S. Ottaviano, A. Peretto, and N. Torricelli, "Application and comparison of semi-empirical models for performance prediction of a kW-size reciprocating piston expander," *Appl. Energy*, vol. 249, pp. 143–156, Sep. 2019, doi: 10.1016/j.apenergy.2019.04.070.
[33] W. Li, "Simplified steady-state modeling for hermetic compressors with focus on extrapolation," *Int. J. Refrig.*, vol. 35, no. 6, pp. 1722–1733, Sep. 2012, doi: 10.1016/j.ijrefrig.2012.03.008.
[34] D. M. Aliaga, C. P. Romero, R. Feick, W. K. Brooks, and A. N. Campbell, "Modelling, simulation, and optimisation of a novel liquid piston system for energy recovery," *Appl. Energy*, vol. 357, Mar. 2024, Art. no. 122506, doi: 10.1016/j.apenergy.2023.122506.
[35] G. Zhao, D. Hughes, D. Beynon, Z. Wei, T. Watson, W. C. Tsoi, and J. Baker, "Perovskite photovoltaics for aerospace applications—Life cycle assessment and cost analysis," *Sol. Energy*, vol. 274, May 2024, Art. no. 112602, doi: 10.1016/j.solener.2024.112602.
[36] F. G. Camacho, R. M. Afzal, P. A. L. de Souza, and N. Mahinpey, "Life cycle assessment of different hydrogen production setups from chemical looping reforming system using carburization reactions," *Int. J. Hydrogen Energy*, vol. 73, pp. 63–72, Jul. 2024, doi: 10.1016/j.ijhydene.2024.06.016.

DEGENG ZHAO was born in Hebei, China, in 1995. He received the B.S. degree in process equipment and control from the School of Mechanical and Electrical Engineering, Beijing University of Chemical Technology, Beijing, China, in 2020, where he is currently pursuing the Ph.D. degree in power engineering and engineering thermophysics. His research interests include mechatronics, energy saving of dynamic equipment, modeling, and simulation.

YAO WANG received the Ph.D. degree from Beijing University of Chemical Technology, in 2019. His research interests include intelligent diagnosis of equipment failure mechanisms and energy-saving optimization.

JINJIE ZHANG received the Ph.D. degree from Beijing University of Chemical Technology, in 2014. In 2016, he stayed with the university after the postdoctoral study. He has published more than 20 articles in the field of fault monitoring and diagnosis of reciprocating compressors, won three provincial and ministerial level scientific and technological progress awards, and nine authorized invention patents. His research interests include online monitoring and intelligent diagnosis technology of reciprocating machinery faults.

ZHINONG JIANG is currently a Professor and a Ph.D. Supervisor. He is also the Deputy Director of the Research Center for Diagnosis and Self-Healing Engineering, Beijing University of Chemical Technology, the Executive Director of the Chinese Society of Vibration Engineering, and the Executive Director of the Fault Diagnosis Committee of the Chinese Society of Vibration Engineering. He has published over 100 academic papers in the past five years. He won three provincial and ministerial level scientific and technological progress awards and 18 authorized invention patents. He has undertaken more than ten vertical projects, including National 973, National 863, National Key Research and Development Program, National Defense 973, and National Defense Research, and has undertaken more than ten enterprise projects, such as petroleum and petrochemical. He presided over the research and development of the first online monitoring and diagnosis system for reciprocating compressor units in China and achieved widespread promotion and application.